The Institute of Space and Astronautical Science
Report No. 635, February 1989

On the Simulation Test for the Relative Motion of Separated Sub-Boosters on M-3SII with Nearly Half a Model Vehicle ST-735 and their Motion Analyses Using Inertial Sensors Output

By

Shigeki TSUKAMOTO

(December 15, 1988)

Summary: In the course of development for M-3SII type vehicle which has two relatively large sub-boosters, a possibility of collision between the separated sub-booster and the core-motor was discussed with concern especially in relation to the effect of the core-motor plume. We had a flight simulation test under the conditions specified by the similarity law given in this paper with ST-735, nearly half a scale model of M-3SII, and the relative motion of the sub-booster was analyzed with on board TV, inertial sensors and a measuring device of separation distance.

Although TV pictures provide us with real time, high speed images of the sub-booster, only 2 dimensional information is obtained in principle. Analysis on the motion with 12 inertial sensors informs us of a complete 3 dimensional motion of the sub-booster. We could predict from the test that the exhaust plume would not influence on the motion of the separated sub-boosters in M-3SII flight.

SYMBOLS

f_j	function in Eqs. of motion	ω	spin rate
g_j	non dimensional function	ξ, η	single pole coordinate
x_i	variables denoting 6 degrees of freedom	φ, θ, ψ	Euler angle
$\boldsymbol{r}$	position vector	α	angle
$\boldsymbol{a}$	acceleration vector	π_i	non dim. parameter
$\boldsymbol{g}$	gravity acceleration vector	i, j	suffix
$\boldsymbol{l}$	position vector	C	core motor
$\boldsymbol{\omega}$	angular velocity vector = $(\omega_1, \omega_2, \omega_3)$	SB	sub-booster
A	M-3SII	s	sensor
B	ST-735		
N	number of non dim. parameters		time derivative
R	Transformation matrix	*	non dim. time deriv.
		–	non dim. operator

a, l, m, q, x, I, Q given in Chapter 2.

1. INTRODUCTION

A simulation test for confirming the performance of some new technics applied to M-3SII type vehicle was scheduled on nearly half a scale model, ST-735. *[REF. 4]* The purposes of this simulation test were

1) Performance test on separation mechanism for sub-boosters
2) Motion analysis of separated sub-boosters

M-3SII type rocket vehicle has two relatively large (735 mmϕ) sub-boosters attached to the first stage core-motor (1410 mmϕ). They are so large compared with the ones on the previous Mu type vehicle that we had to develop a new separation mechanism. The large separated sub-boosters might collide with the core motor at higher altitude by a strike of the plume from the core motor nozzle. The collision would inevitably cause a fatal result, that is, we had to have a great concern with the motion from the standpoint of flight safety.

In order to grasp the motion of the sub-boosters, newly developed on-board CCD cameras take images of them and they are transmitted to the ground on 9.27 GHz X band microwave. γ ray detectors installed on a sub-booster give us also helpful information on separation distance between the detectors and the γ ray sources attached to the core motor. In addition we can reconstruct 3 dimensional relative motion of the separated sub-booster, to which this paper mainly refers, through 12 inertial sensors. Of them, 3 rate integrating gyroscopes and 3 axis accelerometers are on the core motor, and 3 rate gyroscopes and 3 axis accelerometers are on the sub-booster.

Output of two axis rate gyroscopes on a spin-free platform and another rate gyroscope for control of the platform are processed to give the attitude in the single pole coordinate system by 3 on-board microprocessors. Attitude information from the sub-booster, on the other hand, consists of direct output of the rate gryo sensors. Accelerometers are of strain gauge type. The same kind of inertial sensors were installed on both vehicle, M-3SII & ST-735. We visualized the relative motion of separated sub-booster at the post flight analysis using output of these sensors and the results were compared with that using TV images and measurement with the γ ray detector.

TV device has, needless to say, an advantage of real time visualization and our on-board TV device has abilities of high time and spatial resolution. *[REF. 1,2,3]* Since real time close images of the vehicle contain valuable information on the flight conditions, the device helps us to judge in range safety operation. Though our motion analysis with the inertial sensors has, by no means, ability of real time processing, it provides us 3 dimensional motion. Side views of the motion are especially important because we can see by the picture the effect of the exhaust plume.

We had the simulation flight on 17 Jan. 1984. It clarified the motion

of the separated sub-boosters. No problem was observed at all, as TV images shows in Photo, concerning to the relative motion of the separated sub-boosters. Inertial sensors output and the γ ray detector also support it.

Thus, one of the technical obstacles having been resolved, our program, the interplanetary mission to the comet Halley with the vehicle M-3SII was executed and it proved to be successful. The separation was normal, as Fig. 4 shows, as we had predicted from the simulation test.

We will state a similarity law applied to the relative motion of the separated sub-booster in the next chapter, and then will provide results of motion analysis by on-board TV and inertial sensors in later chapters.

2. Similarity Law for Motion of the Separated Sub-Booster

First we define symbols A, B, which denote the simulated and the simulating vehicle as,

A; M-3SII
B; ST-735 .

We assume that the sub-booster keeps to be rigid through the process. So the motion can be expressed by 6 variables (x_1, x_2, x_3, x_4, x_5, x_6) corresponding to the degree of freedom.

In addition to the assumption above we will have further assumptions as follows,

Assumptions:

For both vehicle A & B,

1) The contour of A and B are geometrically similar. The similarity holds not only for rigid contours but also for the boundary of core motor plume.

2) For the supersonic region $2.4 < M < 3.2$ any aerodynamic coefficient is a function of the form of a vehicle only.

3) The sub-booster obeys equations of motion and initial conditions of the following form.

Equations of motion;

$$0 = f_j(\ddot{x}_1, \ddot{x}_2, \ddot{x}_3, \ddot{x}_4, \ddot{x}_5, \ddot{x}_6, \dot{x}_1, \cdots, \dot{x}_6, x_1, \cdots, x_6, q, Q, a, \omega, m, I, l, x_{CG}) \quad (j = 1, \cdots, 6),$$

With initial conditions;

$$\dot{x}_i = \dot{x}_{io},\ x_i = x_{io} \qquad (i = 1, \cdots, 6)$$

and further we assume that a solution exists and it is unique.

The definitions of parameters in the equations and their dimensions are given as;

		DIMENSION L	M	T
q	dynamic pressure of ambient flow just after the separation	− 1	1	− 2
Q	dynamic pressure of exhaust plume of the core motor	− 1	1	− 2
a	acceleration of the core motor just after the separation	1	0	− 2
ω	angular velocity of the core motor just after the separation	0	0	− 1
I	moment of Inertia of the sub-booster	2	1	0
m	mass of the burned out sub-booster	0	1	0
l	length of the sub-booster	1	0	0
x_{CG}	position of the center of gravity	1	0	0

The master equations can be transformed into non-dimensional form with non-dimensional variables and parameters by well-known Buckingham's π theorem as,

M. Es

$$0 = g_j(\overset{**}{\overline{x_1}}, \cdots, \overset{**}{\overline{x_6}}, \overset{*}{\overline{x_1}}, \cdots, \overset{*}{\overline{x_6}}, \overline{x_1}, \cdots, \overline{x_6}; \pi_1, \pi_2, \cdots\cdots, \pi_N),\ j = 1, \cdots, 6$$

I.C

$$\overset{*}{\overline{x_i}} = \overset{*}{\overline{x_{io}}}, \qquad \overline{x_i} = \overline{x_{io}} \qquad i = 1, \cdots, 6$$

where the operator $-$ operates the variable x_i and makes it non-dimensional, and the operator * is non-dimensional time differentiation operator defined as

$$* = d/d\bar{t} = (l/a)^{\frac{1}{2}} d/dt$$

We can easily get N as $N = 8-3 = 5$. If we set any π_i of B equals to π of A and any $\overset{*}{\overline{x_{io}}}$ of B equals to $\overset{*}{\overline{x_{io}}}$ of A (the conditions for $\overline{x_{io}}$ are unnecessary if we take the assumption (1)), then we can affirm that $\overline{x_i}$ of A equals to $\overline{x_i}$ of B for any i because a solution exists and it is unique.

In ordinary expression of 6 degree of freedom for a rigid body, three co-ordinates for the center of gravity and Euler angles are taken. According to the definitions of the variables x_i, the non-dimensional variables $\overline{x_i}$ should be defined as follows,

$$\overline{x_i} = x_i/l \ . \qquad \text{for } i = 1, 2, 3$$

Angles are non-dimensional by definition, so we can define as,

$$\overline{x_i} = x_i \quad . \qquad \text{for } i = 4, 5, 6$$

It should be pointed out here that traces of the center of gravity of B is similar to that of A and the similarity ratio is l_B / l_A. Attitude angles are also similar, or we should say they are always the same at corresponding time. The similarity ratio for time is given as $\sqrt{a_A l_B / a_B l_A}$.

The non-dimensional similarity parameters ($i = 1, \ldots, 5$) are expressed as follows,

$$\pi_1 = \frac{ql^2}{ma} \quad \pi_2 = \frac{Ql^2}{ma} \quad \pi_3 = \frac{\omega^2 l}{a} \quad \pi_4 = \frac{I}{ml^2} \quad \pi_5 = \frac{x_{CG}}{l}$$

The non-dimensional initial conditions are

$$(\overset{*}{\overline{x_i}})_{t_{sep}} = \left[(l/a)^{\frac{1}{2}} \, dx_i / dt \right]_{t = t_{sep}}$$

Uniqueness of solution holds even if a solution intrudes into the inner region of the boundary of plume. So we can apply the similarity law to the motion of the sub-booster not only in the air stream region (Fig. 1) but also in the plume region. This speculation guarantees effectiveness of our experiment, that is to know the motion of the sub-booster disturbed by a strike of the plume in intruding into the plume region.

We can affirm that if sub-boosters do not collide with the core motor in ST-735 flight, we need not worry about the collision in M-3SII flight at least theoretically.

In the last of this chapter we introduce how the non dimensional parameters were set in ST-735 flight. Important elements and non-dimensional parameters for both vehicles are listed in Table.

The separation time was set such that $\pi_{1,A} = \pi_{1,B}$ by computing time varying parameters in numerical calculation of the trajectory.

Thrusters at the tip of 4 fins have a role of control in roll so as to keep the roll rate zero during flight. Thus the target value of π_3 is zero.

Sub-boosters on ST-735 were designed in consideration of the conditions for $\pi_{4,B}$ and $\pi_{5,B}$ but they are not in good agreement with $\pi_{4,A}$ and $\pi_{5,A}$ partly because sub-boosters on M-3SII have heavy device, unit of movable nozzle, at the bottom.

We did not intend to design a new rocket motor satisfying the condition $\pi_{2,B} = \pi_{2,A}$ in favor of the use of an existing rocket motor with 735 mm diameter.

There was no evidence that the non-dimensional initial conditions, which would depend upon flight histories, had a great discrepancy between the two flights.

3. Motion Analysis of the Separated Sub-Booster by On-Board TV Images

In Photo TV images of the motion of the separated sub-booster are given. The motion analysis with the images is shown in Fig. 2. The separation time in this experiment was set to be 21 sec. after the lift-off in considering the conditions given by the similarity law stated in chapter 2.

The CCD camera installed at the frustum of the upper stage, the hammer

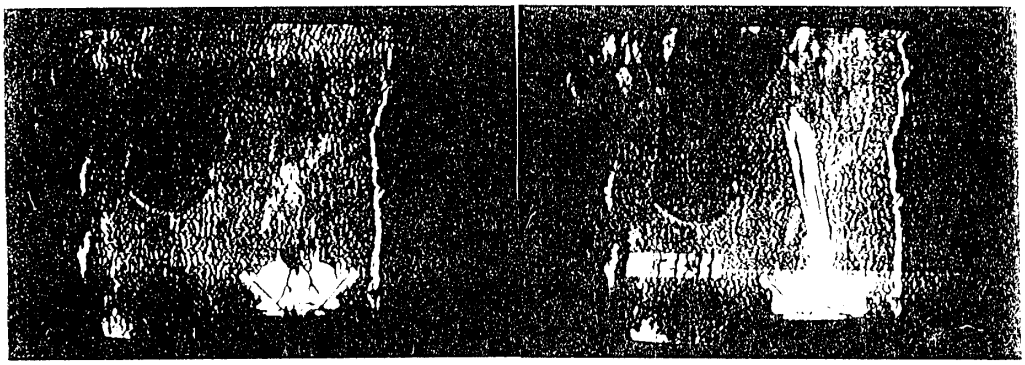

20.00 21.11

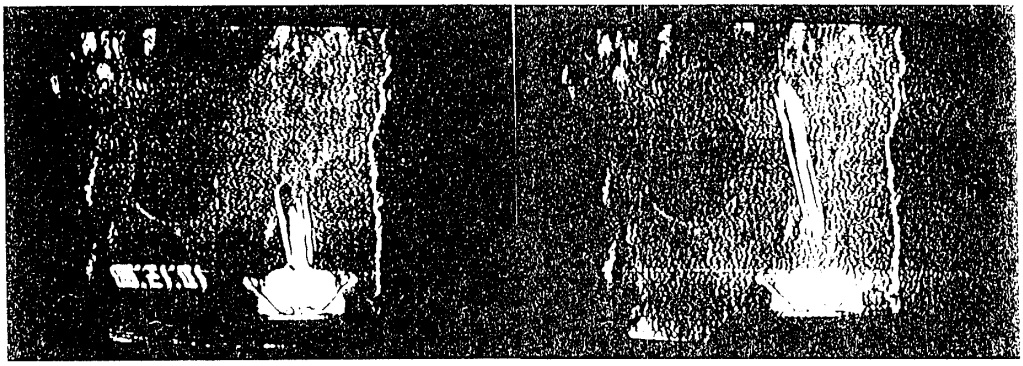

21.01 21.15

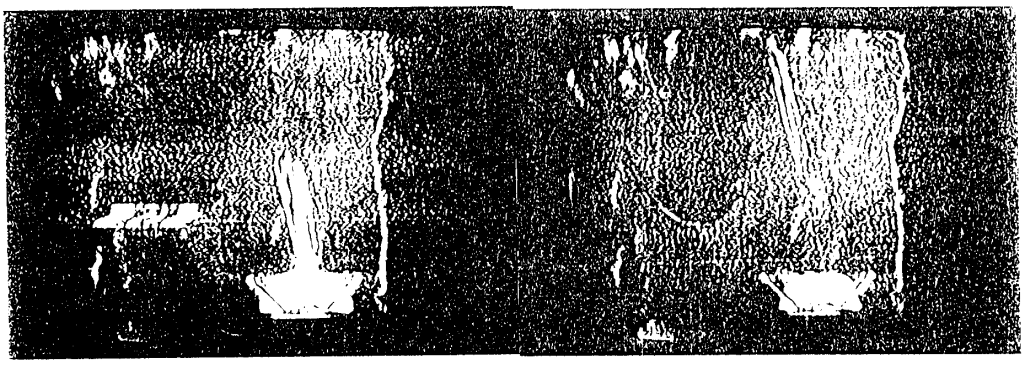

21.06 21.21

Photo TV images on separated sub-booster.

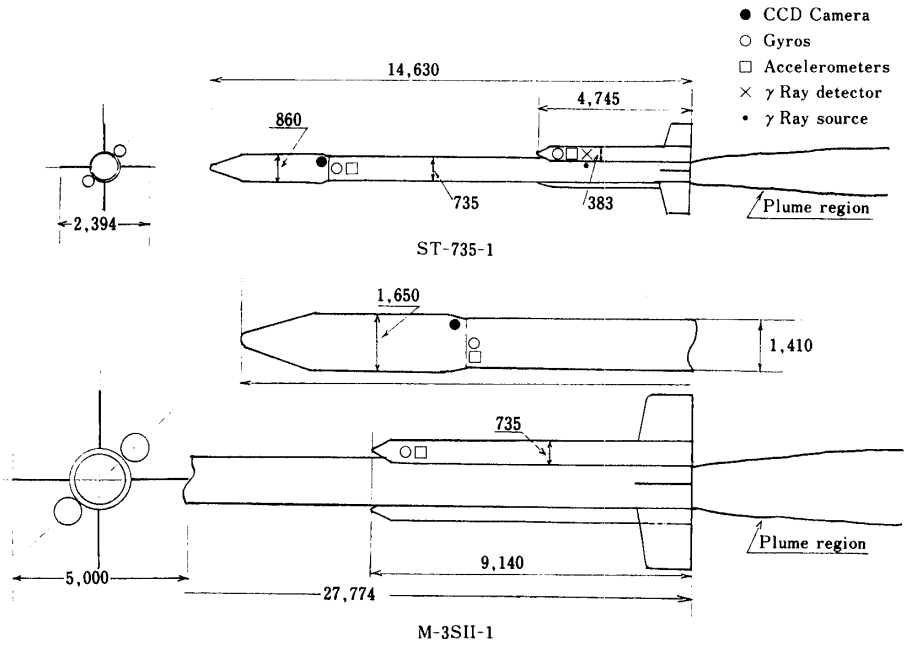

Fig. 1. M-3SII-1 & ST-735.

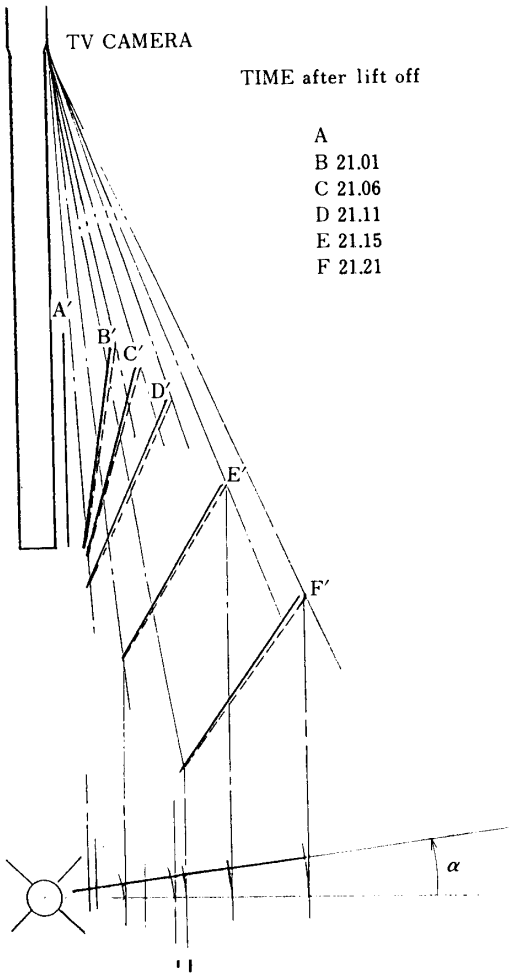

Fig. 2. Relative motion of the sub-booster after separation by TV images.

head part (Fig. 1), looks downward and it has 39.1° H X 29.7°V view angle. The newly developed on-board camera has relatively high time and spatial resolution (20,000 piccel) and (60 frame/sec) *[REF. 1, 2, 3]*.

The carrier signal of X band transmitter is frequency-modulated by the video signal, amplified to 2 watts and then fed to the antenna. The device has an ability to 50 km transmission distance (S/N 45 db). The TV system was improved later and two cameras were installed in M-3SII-2 flight. Each motion of the two sub-boosters was caught separately and signals on both images were mixed and transmitted on Ku band carrier then. *[REF. 1]*

TV images show that the separated sub-booster seems to be confined its motion to a plane obtained by rotating x_1x_2 plane by α in Fig. 2. We drew figures of 3-dimensional motion of the sub-booster using successive TV images under the assumption that its motion is planar. Let us show how the figures are constructed. First let the looking angles measured from the TV

TABLE Elements & non dimensional parameters

	ST-735	M-3SII		
Total length	14,630	27,774	mm	
Diameter Max.	860	1,650	mm	
	735	1,410	mm	
S.B. length	4,745	9,240	mm	
diameter	383	735	mm	
Total weight	7,431	62,215	mm	
S.B. weight	356*2	5,126*2	kg	(ig.)
		1,095*2	kg	(b.o.)
Center of Gravity	8,639	17,025	mm	(ig.)
(C.G.)	7,305	12,026	mm	(b.o.)
S.B. C.G.	2,791	8,639	mm	(ig.)
		7,305	mm	(b.o.)
S.B. I	93.26	10,057	$kgms^2$	(b.o.)
q	16,418	9,218	kg/m^2	
a	43.35	32.93	m/s^2	
expansion ratio	9.1	7.8		
Mach Num.	3.82	3.65		
ratio of sp. heat	1.204	1.204		
chamber Pres.	46	45	kg/cm^2	
Q	1.82	2.25	kg/cm^2	
ω	0	3	deg/s	
PAI 1	235	226		
PAI 2	261	553		
PAI 3	0	$7.6*10^{-4}$		
PAI 4	0.114	0.269		
PAI 5	0.588	0.799		

images for the top and the bottom of the sub-booster are taken at the point where the camera locates. [Fig. 2] With measured diameter of the booster we can take the distances from the camera to the top of the sub-booster. The locations on the angle line are denoted by A', B',$\cdots F'$. As the length of a sub-booster are fixed, each bottom point is set on each bottom line. The dotted lines provide us the moving body central axes in the plane P. A front view and a side view of the motion are drawn by rotating the dotted lines by α. A front view of the motion is shown in real lines below and the side view above.

We can grasp the relative motion of the separated sub-booster at a glance, though the picture has less accuracy than that in Fig. 3.

We also represent the separation distances measured by the γ ray detector on the picture. The device is effective for relatively short distnace. *[REF. 4]*

4. Analysis on Relative Motion of the Separated Sub-Booster Using Inertial Sensors

Now we will have relative motion of a sub-booster after separation by processing the 12 components observation data $\boldsymbol{a}_C$, $\boldsymbol{a}_{SB}$, (φ, θ, ψ), ω_{SB}. As the motion of a rigid body can be expressed by 6 degree of freedom, it is enough in representing the relative motion of the two rigid bodies, the core motor and the sub-booster, to have 12 degrees of freedom.

The equations of translational motion for the two rigid bodies are expressed as;

$$\ddot{\boldsymbol{r}}_C = \boldsymbol{a}_C + \boldsymbol{g}$$
$$\ddot{\boldsymbol{r}}_{SB} = \boldsymbol{a}_{SB} + \boldsymbol{g}$$

where suffix C denotes the core motor and suffix SB denotes the sub-booster. $\boldsymbol{a}$ stands for the acceleration caused by external forces except the gravity force. The accelerations of the center of gravity are obtained from sensor output suffixed by S as

$$\boldsymbol{a}_C = [\boldsymbol{a}_C]_S - \omega_C \times (\omega_C \times \boldsymbol{r}_{C,S})$$
$$\boldsymbol{a}_{SB} = [\boldsymbol{a}_{SB}]_S - \omega_{SB} \times (\omega_{SB} \times \boldsymbol{r}_{SB,S})$$

By subtracting equations above we have the relative acceleration as

$$\boldsymbol{a} = \ddot{\boldsymbol{r}}_{SB} - \ddot{\boldsymbol{r}}_C = \boldsymbol{a}_{SB} - \boldsymbol{a}_C$$

Of importance is that the formula does not contain $\boldsymbol{g}$. Relative position vector can be acquired by integrating the acceleration twice with respect to time, so we have

$$\boldsymbol{r} = \boldsymbol{r}_{SB} - \boldsymbol{r}_C = \iint (\boldsymbol{a}_{SB} - \boldsymbol{a}_C)\, dt$$

As we are going to have relative motion of the sub-booster with respect to the core motor, it is natural to express $\boldsymbol{r}$ in the core motor fixed coordinate. Though our rate integrating gyroscopes provide us attitude of the core motor in single pole representation, we choose the traditional formulation, in Euler representation.

We define pitch angle φ, yaw angle θ and roll angle ψ in the following order as;

$$[\boldsymbol{e}_{1F}, \boldsymbol{e}_{2F}, \boldsymbol{e}_{3F}] \xrightarrow{\varphi}\text{(in pitch)}\xrightarrow{\theta}\text{(in yaw)}\xrightarrow{\psi}\text{(in roll)}---[\boldsymbol{e}_1, \boldsymbol{e}_2, \boldsymbol{e}_3]$$

Transformation matrix R defined by above rotations is given in the form of

$$\begin{aligned} R &= T(\varphi)\,T(\theta)\,T(\psi) \\ &= \begin{pmatrix} 1 & 0 & 0 \\ 0 & \cos\varphi & \sin\varphi \\ 0 & -\sin\varphi & \cos\varphi \end{pmatrix} \begin{pmatrix} \cos\theta & 0 & -\sin\theta \\ 0 & 1 & 0 \\ \sin\theta & 0 & \cos\theta \end{pmatrix} \begin{pmatrix} \cos\psi & \sin\psi & 0 \\ -\sin\psi & \cos\psi & 0 \\ 0 & 0 & 1 \end{pmatrix} \end{aligned}$$

On the other hand transformation matrix R is presented in single pole representation as

$$R=\frac{1}{1+\xi^2+\eta^2}\begin{pmatrix} 1+\xi^2+\eta^2, & 2\xi\eta, & -2\eta \\ 2\xi\eta, & 1+\xi^2+\eta^2, & 2\xi \\ 2\eta, & -2\xi, & 1-\xi^2-\eta^2 \end{pmatrix}$$

By the matrix relations above two, we have

$$\sin\varphi=\frac{2\xi}{\sqrt{(1-\xi^2-\eta^2)+4\xi^2}},\quad \sin\theta=\frac{2\eta}{1+\xi^2+\eta^2}=\frac{-2\xi\eta}{\sqrt{(1-\xi^2-\eta^2)^2+4\xi^2}}$$

$$\cos\varphi=\frac{1-\xi^2-\eta^2}{\sqrt{(1-\xi^2-\eta^2)+4\xi^2}},$$

$$\cos\theta=\frac{\sqrt{(1-\xi^2-\eta^2)^2+4\xi^2}}{1+\xi^2+\eta^2}=\frac{1+\xi^2-\eta^2}{\sqrt{(1-\xi^2-\eta^2)^2+4\xi^2}}$$

Any component of the transformation matrix for the core motor can be calculated with these relations. We denote a transformation matrix from a inertial reference frame to core motor fixed frame by R_C and a transformation matrix from the reference frame to sub-booster fixed frame by R_{SB}, then they are in the form of

$$R = R(\varphi_C, \theta_C, \psi_C)$$
$$R = R(\varphi_{SB}, \theta_{SB}, \psi_{SB}).$$

where φ_{SB}, θ_{SB}, ψ_{SB} are obtained by integrating the equation

$$\begin{pmatrix} \Delta\varphi_{SB} \\ \Delta\theta_{SB} \\ \Delta\psi_{SB} \end{pmatrix} = \Delta t \begin{pmatrix} 0, \sin\psi_{SB}/\cos\theta_{SB}, \cos\psi_{SB}/\cos\theta_{SB} \\ 0, \quad \cos\psi_{SB}, \quad -\sin\psi_{SB} \\ 1, \tan\theta_{SB}/\sin\psi_{SB}, \tan\theta_{SB}\cos\psi_{SB} \end{pmatrix} \begin{pmatrix} \omega_1 \\ \omega_2 \\ \omega_3 \end{pmatrix}$$

with the conditions $\varphi_{SB} = \varphi_0$, $\theta_{SB} = \theta_0$ and $\psi_{SB} = \psi_0$.

The succession of two rotational transformation $R_{SB}^{-1} \times R_C$ and $R_C \times R_{SB}^{-1}$ are also rotational transformation and the latter gives a transformation of any vector component in sub-booster fixed coordinate into the core motor fixed coordinate.

We denote a position vector of the nose tip by $\boldsymbol{l}_N$ and that of tail by $\boldsymbol{l}_T$. These vectors and the relative position vector are transformed in the core motor coordinate as

$$R_C R_{SB}^{-1} \boldsymbol{l}_N, \; R_C R_{SB}^{-1} \boldsymbol{l}_T$$
$$\boldsymbol{r} = \int\int (R_C R_{SB}^{-1} \boldsymbol{a}_{SB} - \boldsymbol{a}_C)\, dt$$

The latter equation gives a position of sub-booster's center of gravity and the former equations give the locations of the nose and the tip with respect to it. Our purpose is fulfilled.

5. Experimental Results

First we give specifications of our inertial sensors. Rate integrating gyroscopes installed on the core motor perform within 2 degree/H gyrodrift under non g sensitive condition. Rate gyroscopes installed on the sub-booster allow angular velocity up to +110 deg/sec. Sub-booster borne strain gauge type accelerometers have measuring range of ±15 g, on the other hand, core motor borne accelerometers have narrower range, ±2.5 g in lateral directions, +20 g ~ −5 g in longitudinal direction.

Fig. 3 represents 3 dimensional motion of the separated sub-booster in the simulation test on ST-735. Green lines show the relative position of the booster's central axis in every 5 msec. Red lines give the position in every 100 msec. The relative positions later than 300 msec after the separation are not given because of a scale over in the lateral accelerometer. The sub-booster departs in accelerated way from the core motor, as the illustration

shows, not only in longitudinal direction but also in lateral direction and this signifies generation of lift force for the booster. The lateral movement avoids a danger of collision induced by the core motor plume. TV images also give the lateral movement. The front view right shows that the sub-booster flew out not in normal direction but with an angle α .

In Fig. 4. 3 dimensional motion of the separated sub-booster in M-3SII-1 flight is presented. Numerical integration was performed from 40.000 sec to 40.800 sec after the ignition with integration time interval 5 msec. The actual separation time is considered to be 40.152 sec by interpreting axial accelerometer data. It is easily recognized that the separated sub-booster departs in slower motion than that in the simulation test. The slower motion is, of course, due to the fact that time scale is longer by the factor of $\sqrt{a_B l_A / a_A l_B}$ as given in chapter 2. The sub-booster also moves in accelerated way not only in longitudinal direction under inertial force and the air drag force but in lateral direction under the lift force just shown in the side view. We can recognize the colliolis effect for the sub-booster shown in the front view, but the effect remains to be small.

It may be said that the speculation stated above are more comprehensive through visualization of 3 dimensional motion in processing 12 inertial sensors, comparing to the data analysis on TV images which are essentially 2 dimensional.

There is no danger at all for the M-3SII-1 sub-booster, as shown in these pictures, of submerging into the exhaust plume, which we predicted in the simulation test.

CONCLUSION

1) Analyses on the relative motion of the separated sub-booster are given. By processing 12 inertial sensors output, we reconstructed the motion of the sub-boosters for the simulation model vehicle ST-735 and the simulated M-3SII vehicle both.

2) We provided the similarity law for the relative motion of the separated sub-boosters. Through it, we could predict from the simulation test that the exhaust plume by the core motor would not influence on the motion of the separated sub-booster in M-3SII flight.

3) The results of motion analysis were compared with that by TV images and γ ray detector.

ACKNOWLEDGEMENT

I would like to express my gratitude to Prof. Matsuo at ISAS who realized me the need for analysis on the motion of separated sub-booster in process-

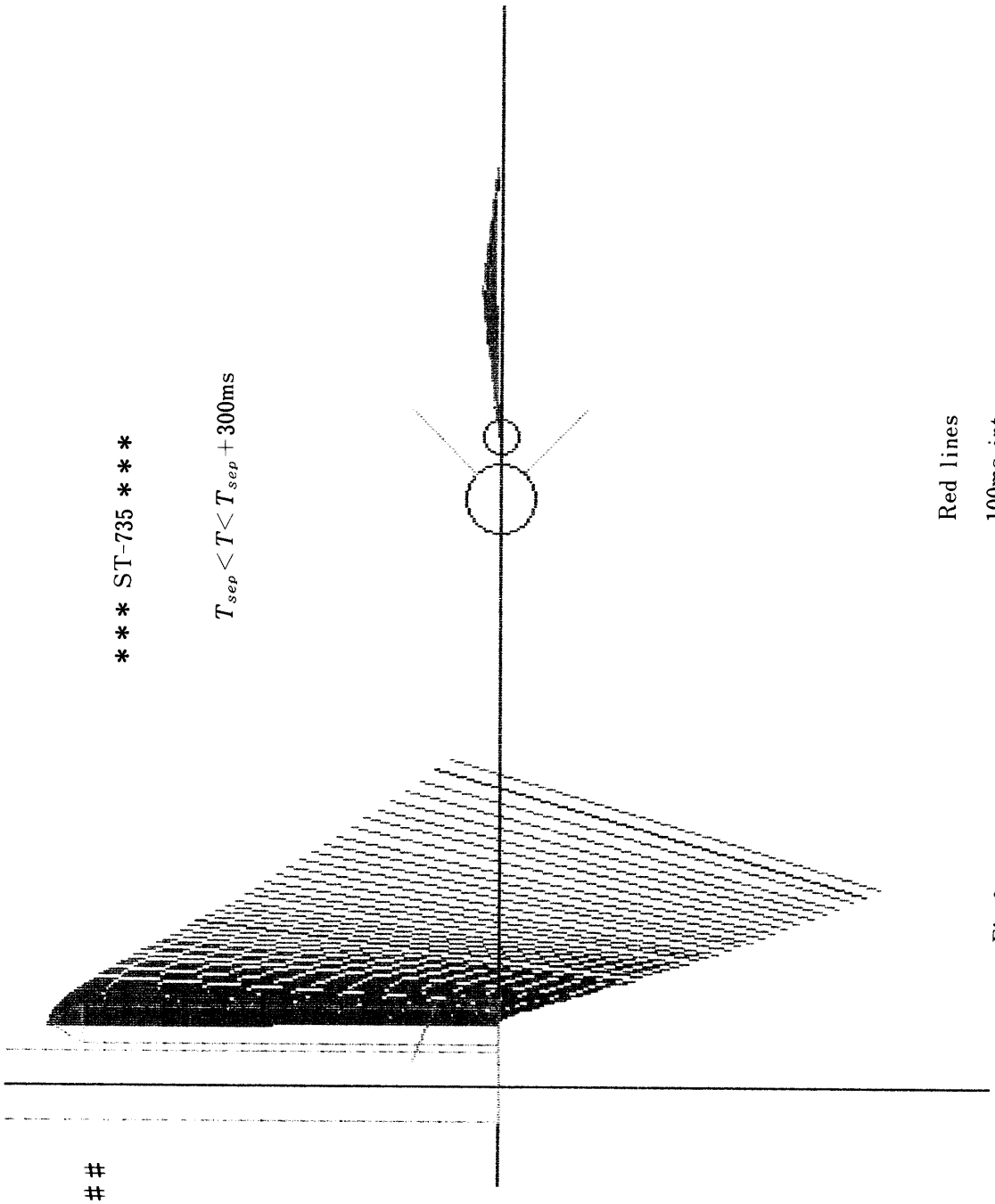

Fig. 3.

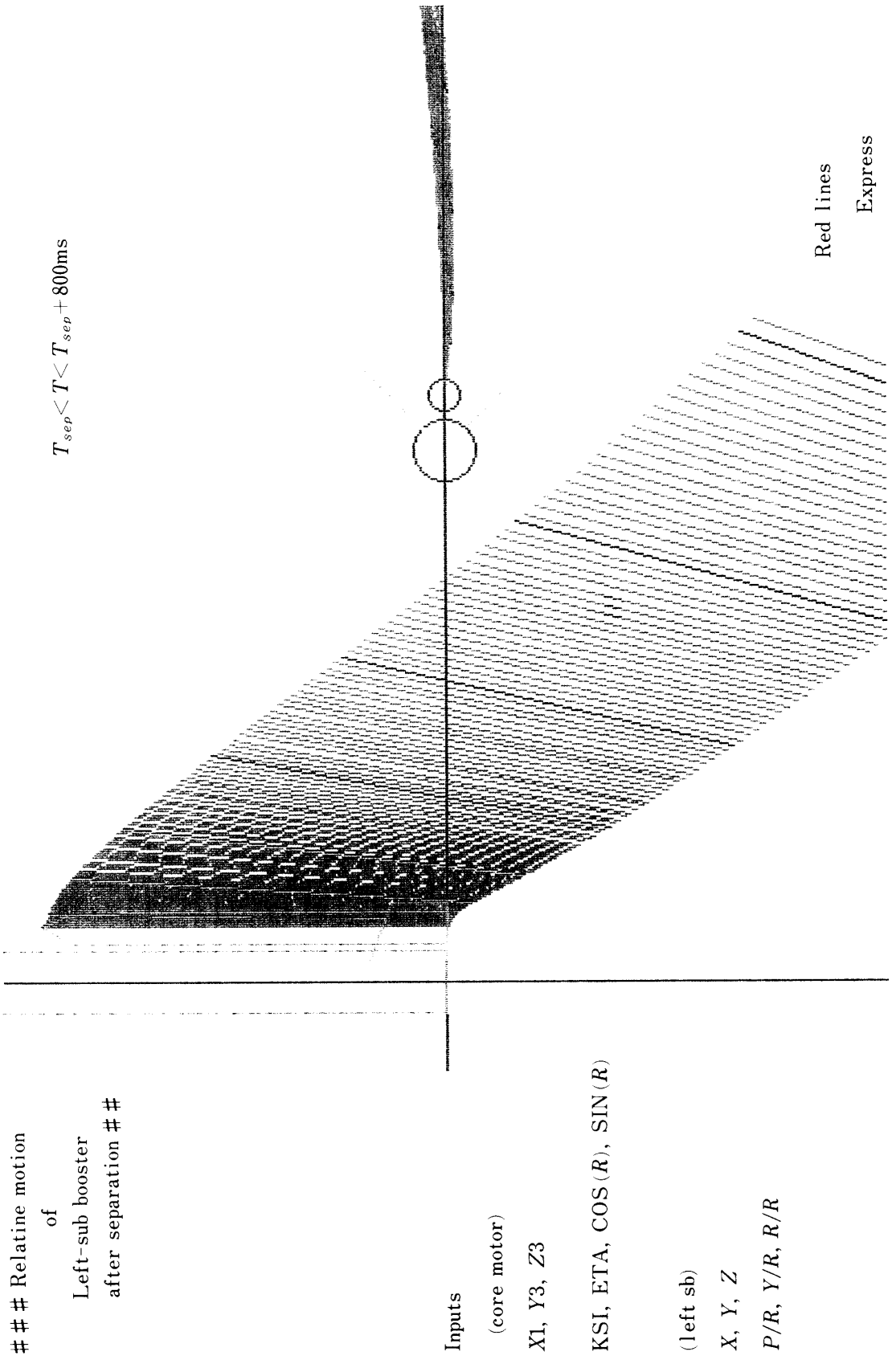

Fig. 4.

ing inertial sensors output. I owe much to Prof. Ogawara who gave me valuable advices on $\dot{\gamma}$ ray detector. Particular appreciations are expressed to Mr. Yokoyama and Mr. Onishi, who worked together in making design of TV devices and preparing for the tests, to Mr. Tange who gave me information on gyroscope data.

REFERENCES

[1] Rocket borne TV image transmission equipment. T. Hayashi, K. Yokoyama, A. Onishi etw. ISAS & NEC, 1986.

[2] Rocket borne X band TV transmission equipment, T. Hayashi, K. Yokoyama, A. Onishi etw. ISAS & NEC, 1985.

[3] Rocket borne TV camera, T. Hayashi, K. Yokoyama, A. Onishi, ISAS, M. Kudoh, S. Obi, M. Kajikawa, T. Kimura, NEC, *Proc. PISSTA*, pp. 724 727, Peking, 1987.

[4] ST-735-1 Flight Program, SES-TD-83-015, ISAS, 1984.

[5] M-3S-II-1 Flight Report, SES-TD-85-008, ISAS, 1985.